Acoustic emissions document stress changes over many seismic cycles in stick-slip experiments

T. H. W. Goebel,[1] D. Schorlemmer,[2] T. W. Becker,[1] G. Dresen,[3] and C. G. Sammis[1]

Received 25 February 2013; revised 19 April 2013; accepted 25 April 2013; published 31 May 2013.

[1] The statistics of large earthquakes commonly involve large uncertainties due to the lack of long-term, robust earthquake recordings. Small-scale seismic events are abundant and can be used to examine variations in fault structure and stress. We report on the connection between stress and microseismic event statistics prior to the possibly smallest earthquakes: those generated in the laboratory. We investigate variations in seismic *b* value of acoustic emission events during the stress buildup and release on laboratory-created fault zones. We show that *b* values mirror periodic stress changes that occur during series of stick-slip events, and are correlated with stress over many seismic cycles. Moreover, the amount of *b* value increase associated with slip events indicates the extent of the corresponding stress drop. Consequently, *b* value variations can be used to approximate the stress state on a fault: a possible tool for the advancement of time-dependent seismic hazard assessment. **Citation:** Goebel, T. H. W., D. Schorlemmer, T. W. Becker, G. Dresen, and C. G. Sammis (2013), Acoustic emissions document stress changes over many seismic cycles in stick-slip experiments, *Geophys. Res. Lett.*, *40*, 2049–2054, doi:10.1002/grl.50507.

1. Introduction

[2] Seismicity provides the most readily available information about crustal stress heterogeneity [*Schorlemmer et al*., 2005; *Narteau et al*., 2009] and stress orientations [*Gephart and Forsyth*, 1984; *Michael*, 1987]. Recent studies of natural and induced microseismicity [*Schorlemmer et al.*, 2004a; *Bachmann et al.*, 2012; *Tormann et al.*, 2012] have drawn from laboratory insights [*Scholz*, 1968; *Main et al*., 1989; *Meredith et al*., 1990; *Lockner et al*., 1991; *Lei et al*., 2000; *Amitrano*, 2003] to interpret spatial *b* value (slope of the frequency-magnitude distribution) variations in terms of crustal stress changes. Increasing stresses in laboratory experiments on intact samples cause *b* values to drop prior to failure. This drop is observed for a range of rock types [e.g., *Main et al.*, 1989; *Thompson et al.*, 2006]. In the Earth's continental crust, low *b* value anomalies have been widely observed, e.g., in California [*Wiemer and Wyss*, 1997; *Wyss et al.*, 2000; *Wyss*, 2001] and also for induced microseismicity with magnitudes down to $M = -4.4$ [*Kwiatek et al.*, 2010]. Regions of low *b* value can be connected to fault-structural heterogeneity and local stress concentrations which cause seismic events to grow to relatively larger sizes once they start to nucleate [*Goebel et al.*, 2012].

[3] While spatial variation in *b* value have already been used to formulate forecasts for large earthquakes ($M \geq 5.0$) in a time-independent sense [*Schorlemmer et al.*, 2004b; *Wiemer and Schorlemmer*, 2007; *Gulia et al.*, 2010], temporal variations in *b* are more controversial, partially due to a lack of long-term, homogeneous earthquake recordings. A recent study suggested that there is no statistically significant predictive power in temporal variations of *b* values, at least for predictions of earthquakes with $M = 4.0–6.2$ [*Parsons*, 2007]. Others, however, view decreasing *b* values as a possible precursor for the occurrence of large earthquakes (i.e., events with $M \gtrsim 6.0$) [*Wyss*, 1990; *Imoto*, 1991; *Nanjo et al.*, 2012]. Part of the current controversy is due to a posteriori observations about phenomena preceding individual seismic events that would not withstand rigorous, statistical testing. Such observations are likely biased because of the intentional search for anomalies. Furthermore, the interpretation of *b* value variations in nature is nonunique due to the intrinsic complexity of the faulting process and the lack of supportive observations, e.g., of stress variations in borehole measurements. This emphasizes the importance of a detailed understanding of the mechanisms behind *b* value variations.

[4] Within the framework of our experiments, we are able to overcome some of these obstacles. We examine physical conditions that cause *b* values to decrease during several seismic cycles on laboratory faults, which cannot readily be done in nature. Despite the inherent difference in scale between laboratory and natural seismicity, several similarities have been highlighted by recent studies. In particular, sample-scale faults in the laboratory show structural similarities to upper crustal faults [*Amitrano and Schmittbuhl*, 2002], and the statistics of laboratory acoustic emission (AE) events exhibit patterns similar to natural seismicity [*Goebel et al.*, 2012].

[5] High-frequency AE events in laboratory tests are associated with the formation of and slip on microcracks. This type of microseismic event activity can be associated with distinct pre-failure stages during loading of intact samples [*Lockner et al.*, 1991; *Lei et al.*, 2000]. The macroscopic failure of intact samples is generally preceded by abruptly increasing AE rates, increasing microseismic moment release, and decreasing Gutenberg-Richter *b* values [*Main et al*., 1989; *Meredith et al*., 1990; *Sammonds et al*., 1992; *Liakopoulou-Morris et al*., 1994]. A possible

Additional supporting information may be found in the online version of this article.

[1]Department of Earth Sciences, The University of Southern California, Los Angeles, California, USA.
[2]Department of Physics of the Earth, German Research Centre for Geosciences (GFZ), Potsdam, Germany.
[3]Department of Geodynamics and Geomaterials, German Research Centre for Geosciences (GFZ), Potsdam, Germany.

Corresponding author: T. H. W. Goebel, The University of Southern California, 3651 Trousdale Pkwy., Los Angeles 90089-0740, CA, USA. (tgoebel@usc.edu)

0094-8276/13/10.1002/grl.50507

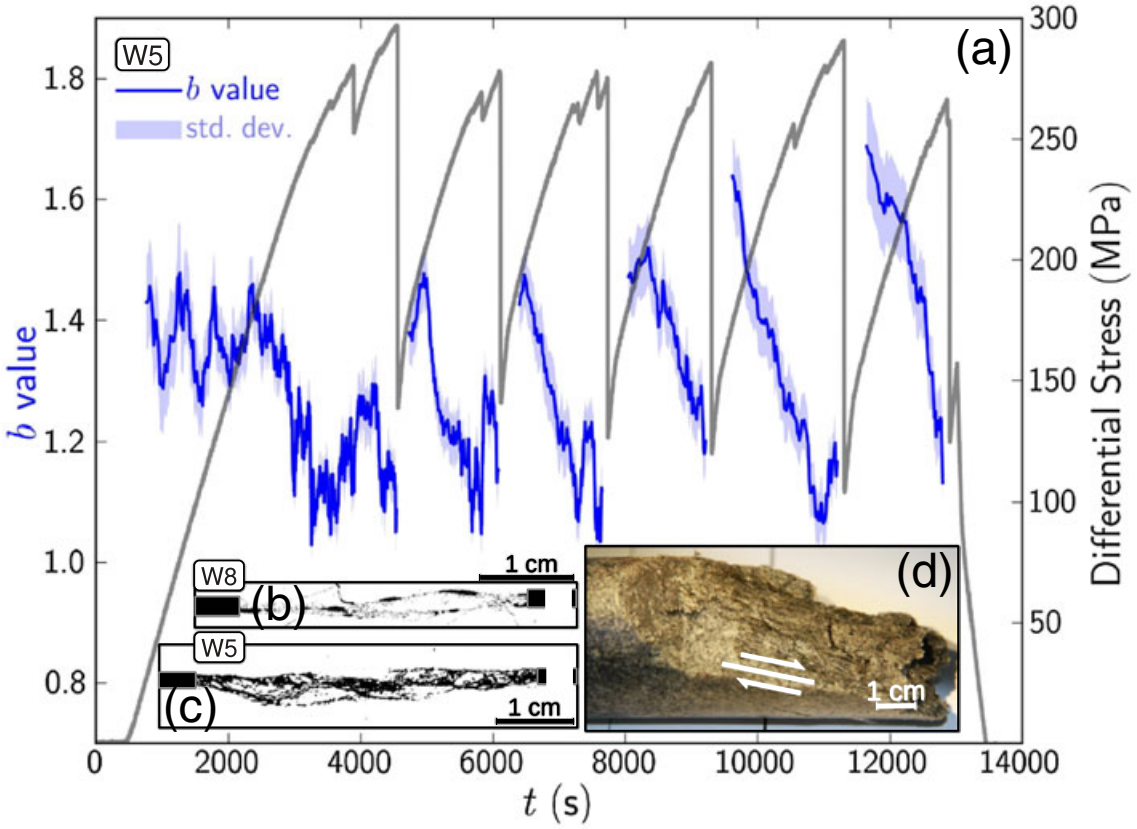

Figure 1. Influence of cyclical stress changes during stick-slip type fault movement on temporal *b* value variations. (a) Both differential stress (gray line) and *b* values (blue line) exhibit a characteristic sawtoothed pattern but with opposite sense (experiment W5). *b* values were computed for 1200 AE sample windows and a 50-event step size. Standard errors in *b* are indicated by blue-shaded areas. (b, c) Post-experimental X-ray computer tomography images of fault zones at the center of the respective samples. The damage zone complexity varied between samples with relatively longer (W5), compared to relatively shorter fracture surfaces (W8). (d) Photographic image of post-experimental slip surface with slip-parallel lineations.

explanation for the connection between *b* and stress is the extension of preexisting microcrack populations by stress corrosion and crack coalescence leading up to the failure of intact samples [*Main et al.*, 1992].

[6] Previous laboratory experiments predominantly focused on macroscopic failure of intact samples or stick-slip motion of planar interfaces. We expand on these experiments through creating structurally complex fault systems starting from incipient fracture surfaces and by documenting variations in stress and AE statistics during series of stick-slip events.

2. Experimental Setup, Methods, and AE Data

[7] In the following, we describe loading conditions and sample geometry which were chosen to represent natural faulting conditions as closely as possible. We report on four triaxial experiments (W4, W5, W7, and W8), conducted on cylindrical (radius = 2 cm, height = 10.7 cm) specimens at constant loading rates $\left(\dot{\epsilon} \sim 3 \cdot 10^{-6}\ \mathrm{s}^{-1}\right)$ at GFZ-Potsdam, Germany. All experiments were performed on oven-dried samples at room temperatures, with constant confining pressures (P_c = 150 MPa). We introduced 1.5–2.5 cm deep saw cut notches at a 30° angle to the loading axis to localize faulting at the center of the specimens during initial fracture and subsequent stick-slip sliding. The results presented here are from the stick-slip sliding stage of previously fractured specimens. Our initial condition, i.e., an incipient fracture surface that develops into a fault zone, can be seen as an analog for the structural complexity of natural fault zones. To monitor microcrack formation and sample deformation, strain gauges and AE sensors were glued to the specimen surface (Figure S1, left, in the supporting information). We employed a high-speed (10 MHz sampling frequency) and accuracy (16 bits amplitude resolution) AE system, enabling the documentation of micromechanical processes that occurred in temporal proximity to slip instabilities. AE events were recorded using a miniature seismic array, consisting of 16 one-component, piezoelectric transducers. The location uncertainty of AE hypocenters was estimated at 1–4 mm, depending on the proximity of the event to the edge of the array. The total number of successfully located AEs from each sample was between 34,141 and 97,847, which allowed robust measurements of *b* value as a function of time. Variations in *b* value were determined using a moving time window that contained an equal number of AE events. This optimized the temporal resolution of *b* value computations while ensuring the same statistical significance of each value. We also scrutinized the effects of different sample sizes and sampling techniques on *b* value trends to ensure reliability and consistency (see supporting information).

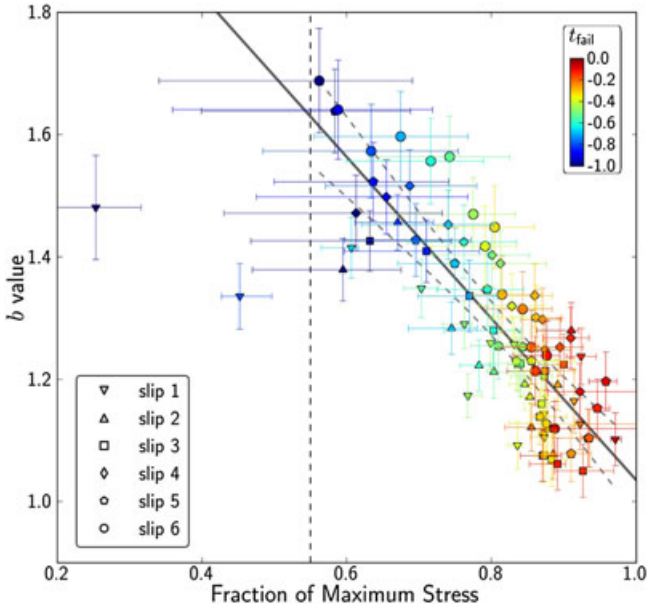

Figure 2. The *b* values drop closer to failure and show an inverse, linear relationship with the differential stress. Depicted are results of all six stick-slips of experiment W5, normalized according to the maximum stress. The markers are colored according to the normalized time to failure (t_{fail}) and the marker symbols indicate individual stick-slip sequences. The curved dashed lines are the 95% confidence bounds of the regression line, and the vertical dashed line shows the 55% limit of the maximum stress used for the linear regression. The horizontal error bars show the extent of the stress window from which AEs were used for *b* value computations. The vertical error bars are the standard error in *b*. For the linear regression using 1200 AE events for each *b* value, we determined a Pearson's *r* of –0.84 which was significant at a 99% level.

3. Results

[8] If *b* value is indeed an indicator of stress [*Schorlemmer et al.*, 2005], we expect to observe a systematic relation between *b* and stress for stick-slip cycles on a fault during our experiments. Figure 1 shows results from experiment W5, which are typical of all experiments. The differential stress shows a characteristic sawtooth pattern pattern of gradual increase followed by an abrupt decrease during slip. At the same time, *b* values decrease with increasing stresses and abruptly increase when the stresses drop during a slip event. The stress curve shows six slip events with large stress drops (LSDs), some of which were preceded by small stress-drop (SSD) events. The loading curve preceding the first three LSD events exhibits many SSDs. The *b* value curves also show more fluctuations during these early cycles. Fluctuations in *b* are strongest during the first stick-slip cycle and decrease with successive LSDs so that the last three stick periods show a smoother, monotonic decrease. This evolution may be related to progressive fault smoothing, which is also indicated by decreasing residual stresses with successive LSD events.

[9] Figure 2 shows *b* as a function of normalized stress (fraction of maximum stress) for the six LSD events in experiment W5. The relationship between *b* and stress is approximately linear for high differential stresses above ≈55% of the peak stress. Below this value, only few AE events were observed and *b* values tend to show more scatter. This scatter is likely related to AEs that occurred due to the reduction of pore space at the initial stage of a loading cycle.

[10] The three other experiments confirmed the relationship between *b* value and stress (Figure S5). This relationship was most pronounced for experiment W8 whereas experiment W4 showed the smallest change in *b* value with larger applied stresses and the scatter in *b* value was comparably large. The scatter at elevated stresses in Figure 2 and during the other experiments may be related to larger fluctuations in *b* associated with geometric complexity especially before the initial LSD events of an experiment.

[11] We also investigated if *b* values carry additional information during high-stress regimes, for example, about the amount of stress release connected to SSD or LSD events. We estimated the stress-drop-related increases in *b* value from the difference between minimum before and maximum *b* value after a stress-drop event. The SSD events produced relatively smaller increases in *b* while LSD events caused a larger upward jump in *b* values (Figure 3). On average, the *b* value jumps are higher for larger stress drops and exhibit a positive correlation with a Pearson's correlation coefficient of $r = 0.64$ for a sample size of $N_{AE} = 600$. We explored this correlation over a range of sample sizes ($r = 0.53$ for $N_{AE} = 300$, $r = 0.57$ for $N_{AE} = 1200$, and $r = 0.57$ for $N_{AE} = 3000$) confirming the connection between *b* increases and stress drops. Furthermore, we tested if this relation is also observed for shear stress drops which were computed for the effective fracture surface area, corrected for slip after each successive slip event [*Scott et al.*, 1994; *Tembe et al.*, 2010]. The linear

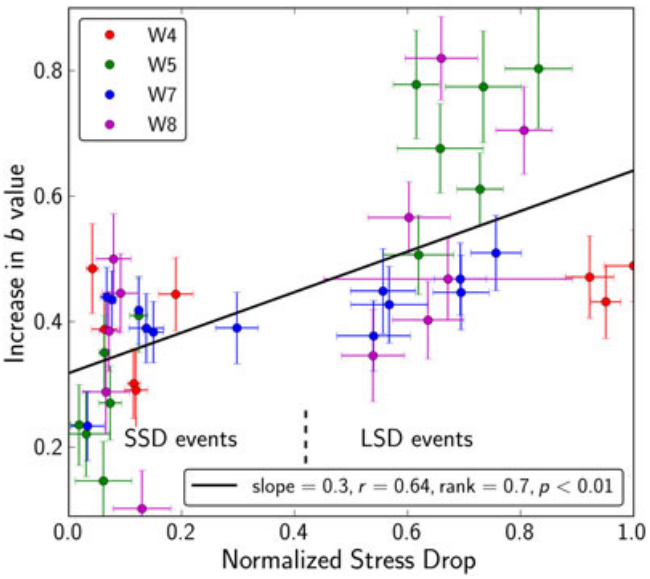

Figure 3. The *b* value increase as function of connected stress drop for all experiments (see upper left legend for marker symbols). Stress drops and *b* value increase showed a linear correlation with Pearson's $r = 0.64$ (Spearman's rank = 0.7) which was significant on a 99% level. Error bars show statistical error in *b* value estimates and the stress range that corresponds to the AE samples used for *b* value computations.

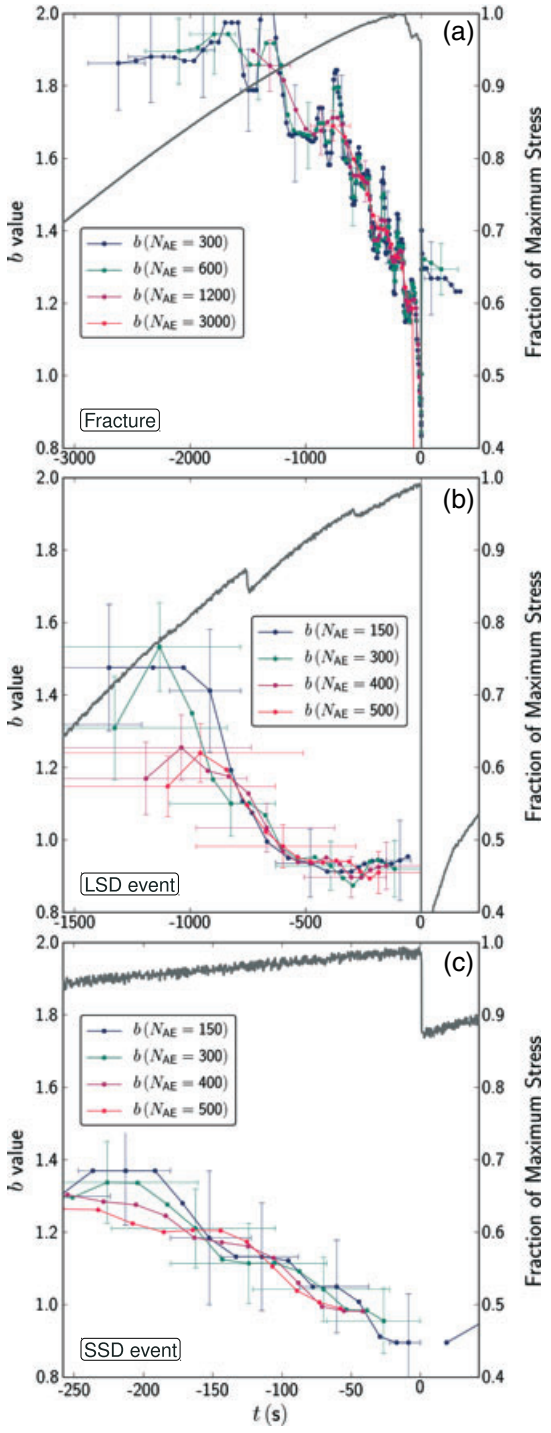

Figure 4. Comparison between *b* value decrease preceding the initial fracture of an intact sample and *b* value decrease in the neighborhood of a large asperity on a natural fault surface. *b* values showed a characteristic decrease (a) before the fracture of the intact sample and before the occurrence of a (b) LSD as well as a (c) SSD. The depicted LSD event corresponds to stick-slip event 5 of experiment W5 shown in Figure 1. *b* value curves for the LSD and SSD event were computed based on AE events that were connected to an asperity region (see text for details). Stresses are normalized to peak stress of individual failure events.

regression between slip-corrected shear stress drop and *b* value increase was characterized by a correlation of $r = 0.65$ which was significant at a 99% level. Thus, the amount of increase in *b* after slip appears to be related to the stress release due to slip.

[12] Assuming that the number of SSD events can serve as a proxy for the degree of structurally related complexity, we performed a systematic analysis of the connection between geometric complexity and *b* value variations. Stick-slip events that were preceded by fewer SSDs showed higher linear correlation coefficients between *b* and stress (Figure S8), consistent with the hypothesis that *b* value-stress relations are more pronounced for structurally less complex faults. Additionally, the times of *b* value minima were closer to the LSD for stick-slips with fewer SSDs (Figure S7). The *b* value-stress relations depended also on the lengths of the laboratory faults, i.e., they were less linear for longer faults (Figure S5). This is consistent with our observation that longer fracture surfaces showed more structural complexity in post-experimental X-ray computer tomography scans (Figures 1b and 1c), and structural complexity can obscure *b* value-stress relations.

[13] To investigate the importance of observational scales on the *b*-stress relation, we compared results from a LSD with a SSD event as well as with the failure of an intact sample (Figure 4). For the LSD and SSD event, we limited our observations to one dominant asperity region within the laboratory-created fault zone, identified through areas of low *b* value, high seismic moment, and large AE density gradients [*Goebel et al.*, 2012]. The temporal variations of *b* values based solely on AEs within asperity regions in Figure 4 show a clear monotonic decrease with increasing stresses before both SSD and LSD event, similar to the fracture of the intact sample, but on a different time scale. The previously observed variations in *b* on short time scales before the LSD events, which seemed to be connected to SSD events (see Figure 1), have largely disappeared, presumably because the SSD events occurred outside the asperity area under study. The similarity in the temporal evolution of *b* value before an initial fracture and the fracture of a single asperity suggests that the underlying micromechanical processes are similar. The additional complexity observed during slip on a rough fault plane is probably due to fault-structural heterogeneity.

4. Discussion and Conclusion

[14] It is commonly assumed that *b* values are stable in time and only reflect spatial variations in stress [*Wiemer and Wyss*, 1997; *Westerhaus et al.*, 2002; *Schorlemmer and Wiemer*, 2005; *Parsons*, 2007]. We observed that *b* values vary significantly within a seismic cycle in stick-slip experiments and that the amount of increase in *b* after a slip event is related to the stress drop (or the equivalent residual stress state on the fault after slip). This is consistent with a recent study of changes in *b* value following the 1989 *M*6.9 Loma Prieta and the 2004 *M*6.0 Parkfield event which suggested that a rapid return of *b* values to pre-failure levels indicates that the local stress field has not been reset and stresses quickly return to pre-failure levels [*Tormann et al.*, 2012]. Our results suggest that the magnitude of increase in *b* value after failure can be associated with the effectiveness of a large earthquake to release stored shear stress on a fault. Relatively small amounts of stress release during a

seismic event could possibly be caused by large structural heterogeneity within a fault zone.

[15] The observed connection between decreasing *b* values and increasing differential stresses substantiates previous findings of a *b* value-stress dependence [*Scholz*, 1968; *Amitrano*, 2003; *Schorlemmer et al.*, 2005]. Our results are also in agreement with a stochastic model that explores variations of the Gutenberg-Richter relationship in the context of an inhomogeneous medium [*Scholz*, 1968]. This model predicts that *b* value is inversely related to the applied stress so that seismic events have a higher probability to grow to larger sizes if the stress level in the medium is high. Consequently, we also expect that an increase in the stress level on the fault, for example, by changing the fault angle or increasing the confining pressure would lead to a general decrease in *b* value. The role of increasing confining pressures in reducing *b* values has been shown during fracture and successive frictional sliding of granite samples [*Amitrano*, 2003].

[16] Our results provide an explanation for the observed decrease in *b* value in the source regions prior to large earthquakes [*Nanjo et al.*, 2012]. We suggest that the underlying physical processes governing *b* value variations affect *b* values on different time scales and over different fault volumes. Disregarding the importance of temporal and spatial scales may lead to a loss of physically driven *b* value variations. *b* values are more strongly correlated with stress for faults with less structural complexity and stick-slip sequences with simple, monotonic stress curves, i.e., without SSD events. This suggest that *b* value-stress relations depend on fault complexity and are more strongly connected for smoother fault surfaces.

[17] Natural faults are likely to contain additional complexity that cannot readily be explored within the framework of the current set of experiments. Our results suggest that this complexity could partially be reduced by choosing an adequate subscale of a fault volume for the analysis of temporal *b* value variations, providing a possible means to explore the relative stress state of a fault segment and its position within the seismic cycle. Furthermore, a detailed understanding of temporal *b* value variations is important for intermediate and long-term earthquake forecasting efforts, especially time-dependent forecast models for hazard assessment.

[18] **Acknowledgments.** We thank Stefan Gehrmann and Matthias Kreplin for rock sample preparation at GFZ-Potsdam, Germany. We thank R. Shcherbakov and an anonymous reviewer for comments that helped improve the manuscript. This research was supported in part by the Southern Californian Earthquake Center under contribution 11017 and 13022.

[19] The Editor thanks Robert Shcherbakov and an anonymous reviewer for their assistance in evaluating this paper.

References

Amitrano, D. (2003), Brittle-ductile transition and associated seismicity: Experimental and numerical studies and relationship with the *b* value, *J. Geophys. Res.*, *108*, 2044, doi:10.1029/2001JB000680.

Amitrano, D., and J. Schmittbuhl (2002), Fracture roughness and gouge distribution of a granite shear band, *J. Geophys. Res.*, *107*, 2375, doi:10.1029/2002JB001761.

Bachmann, C. E., S. Wiemer, B. P. Goertz-Allmann, and J. Woessner (2012), Influence of pore-pressure on the event-size distribution of induced earthquakes, *Geophys. Res. Lett.*, *39*, L09302, doi:10.1029/2012GL051480.

Gephart, J. W., and D. W. Forsyth (1984), An improved method for determining the regional stress tensor using earthquake focal mechanism data: Application to the San Fernando Earthquake Sequence, *J. Geophys. Res.*, *89*(B11), 9305–9320, doi:10.1029/JB089iB11p09305.

Goebel, T. H. W., T. W. Becker, D. Schorlemmer, S. Stanchits, C. Sammis, E. Rybacki, and G. Dresen (2012), Identifying fault heterogeneity through mapping spatial anomalies in acoustic emission statistics, *J. Geophys. Res.*, *117*, B03310, doi:10.1029/2011JB008763.

Gulia, L., S. Wiemer, and D. Schorlemmer (2010), Asperity-based earthquake likelihood models for Italy, *Ann. Geophys.*, *53*(3), 63–75, doi:10.4401/ag-4843.

Imoto, M. (1991), Changes in the magnitude–frequency *b*-value prior to large ($M \geq 6.0$) earthquakes in Japan, *Tectonophysics*, *193*(4), 311–325.

Kwiatek, G., K. Plenkers, M. Nakatani, Y. Yabe, and G. Dresen (2010), Frequency-magnitude characteristics down to magnitude –4.4 for induced seismicity recorded at Mponeng gold mine, South Africa, *Bull. Seismol. Soc. Am.*, *100*, 1165–1173.

Lei, X., K. Kusunose, M. Rao, O. Nishizawa, and T. Satoh (2000), Quasi-static fault growth and cracking in homogeneous brittle rock under triaxial compression using acoustic emission monitoring, *J. Geophys. Res.*, *105*, 6127–6139.

Liakopoulou-Morris, F., I. G. Main, B. R. Crawford, and B. G. D. Smart (1994), Microseismic properties of a homogeneous sandstone during fault nucleation and frictional sliding, *Geophys. J. Int.*, *119*(2), 219–230, doi:10.1111/j.1365-246X.

Lockner, D., J. Byerlee, V. Kuksenko, A. Ponomarev, and A. Sidorin (1991), Quasi-static, fault growth and shear fracture energy in granite, *Nature*, *350*, 39–42.

Main, I. G., P. G. Meredith, and C. Jones (1989), A reinterpretation of the precursory seismic *b*-value anomaly from fracture mechanics, *Geoph. J. Int.*, *96*, 131–138.

Main, I. G., P. G. Meredith, and P. R. Sammonds (1992), Temporal variations in seismic event rate and *b*-values from stress corrosion constitutive laws, *Tectonophysics*, *211*, 233–246.

Meredith, P. G., I. G. Main, and C. Jones (1990), Temporal variations in seismicity during quasi-static and dynamic rock failure, *Tectonophysics*, *175*, 249–268.

Michael, A. J. (1987), Use of focal mechanisms to determine stress: A control study, *J. Geophys. Res.*, *92*, 357–368.

Nanjo, K. Z., N. Hirata, K. Obara, and K. Kasahara (2012), Decade-scale decrease in *b* value prior to the M9-class 2011 Tohoku and 2004 Sumatra quakes, *Geophys. Res. Lett.*, *39*, L20304, doi:10.1029/2012GL052997.

Narteau, C., S. Byrdina, P. Shebalin, and D. Schorlemmer (2009), Common dependence on stress for the two fundamental laws of statistical seismology, *Nature*, *462*, 642–645, doi:10.1038/nature08553.

Parsons, T. (2007), Forecast experiment: Do temporal and spatial *b* value variations along the Calaveras fault portend $M \geq 4.0$ earthquakes? *J. Geophys. Res.*, *112*, B03308, doi:10.1029/2006JB004632.

Sammonds, P., P. R. Meredith, and P. G. Main (1992), Role of pore fluids in the generation of seismic precursors to shear fracture, *Nature*, *359*, 228–230.

Scholz, C. H. (1968), The frequency-magnitude relation of microfracturing in rock and its relation to earthquakes, *Bull. Seismol. Soc. Am.*, *58*, 399–415.

Schorlemmer, D., and S. Wiemer (2005), Microseismicity data forecast rupture area, *Nature*, *434*, 1086, doi:10.1038/4341086a.

Schorlemmer, D., S. Wiemer, and M. Wyss (2004a), Earthquake statistics at Parkfield: 1. Stationarity of *b*-values, *J. Geophys. Res.*, *109*, B12307, doi:10.1029/2004JB003234.

Schorlemmer, D., S. Wiemer, M. Wyss, and D. D. Jackson (2004b), Earthquake statistics at Parkfield: 2. Probabilistic forecasting and testing, *J. Geophys. Res.*, *109*, B12308, doi:10.1029/2004JB003235.

Schorlemmer, D., S. Wiemer, and M. Wyss (2005), Variations in earthquake-size distribution across different stress regimes, *Nature*, *437*, 539–542, doi:10.1038/nature04094.

Scott, D. R., D. A. Lockner, J. D. Beyerlee, and C. G. Sammis (1994), Triaxial testing of Lopez fault gouge at 150 MPa mean effective stress, *Pure Appl. Geophys.*, *142*, 749–775.

Tembe, S., D. A. Lockner, and T.-F. Wong (2010), Effect of clay content and mineralogy on frictional sliding behavior of simulated gouges: Binary and ternary mixtures of quartz, illite, and montmorillonite, *J. Geophys. Res.*, *115*, B03416, doi:10.1029/2009JB006383.

Thompson, B. D., R. P. Young, and D. A. Lockner (2006), Fracture in Westerly granite under AE feedback and constant strain rate loading: Nucleation, quasi-static propagation, and the transition to unstable fracture propagation, *Pure Appl. Geophys.*, *163*(5-6), 995–1019, doi:10.1007/s00024-006-0054.

Tormann, T., S. Wiemer, and J. L. Hardebeck (2012), Earthquake recurrence models fail when earthquakes fail to reset the stress field, *Geophys. Res. Lett.*, *39*, L18310, doi:10.1029/2012GL052913.

Westerhaus, M., M. Wyss, R. Yilmaz, and J. Zschau (2002), Correlating variations of *b*-values and crustal deformations during the 1990s may

have pinpointed the rupture initiation of the M_w = 7.4 Izmit earthquake of 1999 August 17, *Geophys. J. Int.*, *184*(1), 139–152.

Wiemer, S., and D. Schorlemmer (2007), ALM: An asperity-based likelihood model for California, *Seismol. Res. Lett.*, *78*(1), 134–140, doi:10.1785/gssrl.78.1.134.

Wiemer, S., and M. Wyss (1997), Mapping the frequency-magnitude distribution in asperities: An improved technique to calculate recurrence times? *J. Geophys. Res.*, *102*, 15,115–15,128.

Wyss, M. (1990), Changes of mean magnitude of Parkfield seismicity: A part of the precursory process? *Geophys. Res. Lett.*, *17*, 2429–2432, doi:10.1029/GL017i013p02429.

Wyss, M. (2001), Locked and creeping patches along the Hayward fault, California, *Geophys. Res. Lett.*, *28*, 3537–3540.

Wyss, M., D. Schorlemmer, and S. Wiemer (2000), Mapping asperities by minima of local recurrence time: The San Jacinto-Elsinore fault zones, *J. Geophys. Res.*, *105*, 7829–7844.